

# On the evolution of thermally driven shallow cavity flows

By P. G. DANIELS AND P. WANG

Department of Mathematics, City University, Northampton Square, London EC1V 0HB, UK

(Received 12 March 1993 and in revised form 23 July 1993)

The temporal evolution of thermally driven flow in a shallow laterally heated cavity is studied for the nonlinear regime where the Rayleigh number  $R$  based on cavity height is of the same order of magnitude as the aspect ratio  $L$  (length/height). The horizontal surfaces of the cavity are assumed to be thermally insulating. For a certain class of initial conditions the evolution is found to occur over two non-dimensional timescales, of order one and of order  $L^2$ . Analytical solutions for the motion throughout most of the cavity are found for each of these timescales and numerical solutions are obtained for the nonlinear time-dependent motion in end regions near each lateral wall. This provides a complete picture of the evolution of the steady-state flow in the cavity for cases where instability in the form of multicellular convection does not occur. The final steady state evolves on a dimensional timescale proportional to  $l^2/\kappa$ , where  $l$  is the length of the cavity,  $\kappa$  is the thermal diffusivity of the fluid and the constant of proportionality depends on the ratio  $R/L$ .

---

## 1. Introduction

Flows driven by lateral heating in shallow rectangular cavities are of interest in relation to a number of physical and technological phenomena such as the production of crystals by the gradient freeze technique (Hurle, Jakeman & Johnson 1974), cooling systems for nuclear reactors (Boyack & Kearney 1972), solar energy collectors (Bejan & Rossie 1981) and the dispersion of pollutants in river estuaries (Cormack, Leal & Imberger 1974). In many instances the temporal evolution of the flow is of interest, particularly where this occurs over a long timescale, due either to the large lateral extent of the system or, in a geophysical context, to seasonal or other periodic variations.

Steady two-dimensional flow structures due to lateral heating in shallow rectangular cavities are now fairly well understood, particularly in the linear and mildly nonlinear regimes. In the Oberbeck–Boussinesq approximation the flow depends on three non-dimensional parameters: a Rayleigh number  $R$ , based on the cavity height and the lateral temperature difference, the Prandtl number of the fluid  $\sigma$ , and the aspect ratio of the cavity  $L$  (length/height), which here is assumed large. For Rayleigh numbers  $R \ll L$  the flow throughout the cavity consists of a Hadley cell driven by the constant horizontal temperature gradient set up between the endwalls (Cormack *et al.* 1974). Nonlinear convective effects first become significant in the turning motion near the ends when

$$R_1 = R/L = O(1) \quad (1.1)$$

(Hart 1983*a*; Daniels, Blythe & Simpkins 1987). In the same range the single Hadley cell becomes susceptible to a variety of instabilities (Hart 1972, 1983*b*) and above

certain critical values of  $R_1$  the parallel core flow is replaced by multiple cells. The stationary transverse mode of instability actually forms an integral part of the basic steady motion in the cavity but is limited to Prandtl numbers less than about 0.12 (Daniels *et al.* 1987). Longitudinal stationary and travelling wave instabilities and transverse travelling waves are also possible and become the preferred modes of instability for Prandtl numbers greater than about 0.033 but even at moderate Prandtl numbers are limited to extremely high values of  $R_1$  (Kuo & Korpela 1988) and may be discounted as far as the present investigation is concerned. Here attention is restricted to two-dimensional flow and multicellular motion is not expected to be significant provided  $\sigma \geq 0.12$ . Numerical solutions of the Boussinesq equations governing the nonlinear steady-state turning motion in the end regions have been obtained for low Prandtl numbers by Hart (1983*a*) and for a wider range of Prandtl numbers and for Rayleigh numbers  $R_1$  up to 20 000 by Wang & Daniels (1993). The asymptotic structure of the steady-state solution as  $R_1 \rightarrow \infty$  has been discussed by Daniels (1993).

One of the first rational investigations of transient flow in a rectangular cavity was carried out by Patterson & Imberger (1980) who identified many of the important length, time and velocity scales of the motion, allowing a classification of the various possible flow regimes. A number of interesting features were revealed, including an oscillatory approach to steady state under certain conditions. This oscillatory behaviour has since been confirmed in experiments by Ivey (1984) and Patterson & Armfield (1990) and in numerical simulations by Schladow, Patterson & Street (1989). Much of this work has been concerned with cavities of finite aspect ratio and there appears to have been comparatively little work on the time evolution of flows in shallow cavities where  $L \gg 1$ . The value of analysing the asymptotic structure of the solution in this limit, as opposed to performing numerical simulations at finite values of  $L$ , lies not only in its relevance to the applications mentioned earlier but also in the possibility of obtaining approximate but general solutions over a wide range of parameter space and thereby developing a more complete understanding.

The present study investigates such time-dependent flows analytically and numerically for a cavity with thermally insulated horizontal surfaces and endwalls held at different fixed temperatures. The problem is formulated in §2. The fluid is assumed to be initially at rest with a linear, conductive temperature profile across the cavity for which  $R_1 = O(1)$ . In the absence of instabilities, the evolution of the flow is found to occur on two main non-dimensional timescales. The main core flow develops on a timescale  $t = O(1)$  and is discussed in §3. A more complicated motion is generated in roughly square zones near each end of the cavity and the solution there is discussed in §4, with particular emphasis on the structure that emerges as  $t \rightarrow \infty$ . Numerical solutions of the full Boussinesq equations which govern the end region flow are obtained using a Dufort–Frankel multigrid method and are described in §5. The end-zone behaviour as  $t \rightarrow \infty$  in turn creates a reaction in the core region which then adjusts on a long timescale  $t = O(L^2)$  which is considered in §6. This ultimately leads to the attainment of a steady-state solution throughout the cavity. A discussion of the results and extensions of the theory to incorporate more general initial configurations are given in §7.

## 2. Formulation

A cavity of length  $l$  and height  $h$  occupies the region  $0 \leq x \leq L$ ,  $0 \leq z \leq 1$ , where  $(x, z)$  are Cartesian coordinates non-dimensionalized with respect to  $h$ . The cavity is filled with a fluid of kinematic viscosity  $\nu$ , thermal diffusivity  $\kappa$  and coefficient of

thermal expansion  $\alpha$ . The endwall at  $x = L = l/h$  is maintained at a constant temperature  $\Delta T$  in excess of that at  $x = 0$  and the two horizontal walls  $z = 0$  and  $z = 1$  are perfectly insulated. In the Oberbeck–Boussinesq approximation, time-dependent motion is governed by the equations

$$\frac{\partial \bar{u}}{\partial x} + \frac{\partial \bar{w}}{\partial z} = 0, \quad (2.1)$$

$$\sigma^{-1} \left( \frac{\partial \bar{u}}{\partial t} + \bar{u} \frac{\partial \bar{u}}{\partial x} + \bar{w} \frac{\partial \bar{u}}{\partial z} \right) = -\frac{\partial \bar{p}}{\partial x} + \nabla^2 \bar{u}, \quad (2.2)$$

$$\sigma^{-1} \left( \frac{\partial \bar{w}}{\partial t} + \bar{u} \frac{\partial \bar{w}}{\partial x} + \bar{w} \frac{\partial \bar{w}}{\partial z} \right) = -\frac{\partial \bar{p}}{\partial z} + \nabla^2 \bar{w} + R\bar{T}, \quad (2.3)$$

$$\frac{\partial \bar{T}}{\partial t} + \bar{u} \frac{\partial \bar{T}}{\partial x} + \bar{w} \frac{\partial \bar{T}}{\partial z} = \nabla^2 \bar{T} \quad (2.4)$$

for the velocity field  $(\bar{u}, \bar{w})$ , reduced pressure  $\bar{p}$  and temperature  $\bar{T}$ , which are non-dimensionalized with respect to  $\kappa/h$ ,  $\rho\nu\kappa/h^2$  and  $\Delta T$  respectively, where  $\rho$  is the mean density of the fluid. The time  $t$  is non-dimensionalized with respect to  $h^2/\kappa$ , and the Rayleigh number  $R$  and Prandtl number  $\sigma$  are defined by

$$R = \alpha g \Delta T h^3 / \kappa \nu, \quad \sigma = \nu / \kappa, \quad (2.5)$$

where  $g$  is the acceleration due to gravity. The boundary conditions on the rigid walls of the cavity are

$$\bar{\psi} = \bar{w} = \bar{T} = 0 \quad (x = 0), \quad (2.6)$$

$$\bar{\psi} = \bar{w} = 0, \quad \bar{T} = 1 \quad (x = L), \quad (2.7)$$

$$\bar{\psi} = \bar{u} = \partial \bar{T} / \partial z = 0 \quad (z = 0, 1), \quad (2.8)$$

where  $\bar{\psi}$  is a stream function defined by

$$\bar{u} = \partial \bar{\psi} / \partial z, \quad \bar{w} = -\partial \bar{\psi} / \partial x. \quad (2.9)$$

In §§3–6 the evolution of the flow from an initial state

$$\bar{T} = x/L, \quad \bar{\psi} = \bar{u} = \bar{w} = 0 \quad \text{at} \quad t = 0 \quad (2.10)$$

is considered. Because this state is centrosymmetric (Gill 1966) the time-dependent motion that ensues can also be assumed centrosymmetric:

$$\bar{T}(x, z, t) = 1 - \bar{T}(L - x, 1 - z, t), \quad (2.11)$$

$$\bar{\psi}(x, z, t) = \bar{\psi}(L - x, 1 - z, t), \quad (2.12)$$

$$\bar{p}(x, z, t) = R(z - \frac{1}{2}) + \bar{p}(L - x, 1 - z, t), \quad (2.13)$$

allowing only one half of the flow domain to be considered. It will also be assumed that the Rayleigh number and aspect ratio are such that  $R_1 = R/L = O(1)$ , giving rise to a nonlinear motion in the end regions of the cavity.

The initial state (2.10) corresponds to a motionless fluid subjected to a linear lateral temperature variation consistent with the temperatures of the endwalls at  $x = 0$  and  $x = L$ . This conductive state might arise following a sudden increase in the Rayleigh number or as a result of differential thermal radiation of the fluid layer. It could also be produced by internal heating or by thermal conduction on an order-one timescale following differential heating along the horizontal surface of the cavity. The latter

would also produce transient motion that would modify the evolution of the flow on a timescale  $t = O(1)$ , to be considered in §§3–5 below, but would not affect the subsequent long-timescale evolution when  $t = O(L^2)$  to be described in §6. Extensions of the present theory to include a wider class of initial configurations are considered in §7.

### 3. Core region

In the core region away from the endwalls it is appropriate to use as independent variables

$$\xi = x/L, \quad z = z \quad (3.1)$$

and in this section the solution is considered for times  $t = O(1)$ . In the limit as  $L \rightarrow \infty$  it is found that the solution proceeds in inverse powers of  $L$ :

$$\left. \begin{aligned} \bar{T} &= \xi + L^{-1}\tilde{T}(\xi, z, t) + \dots, \\ \bar{\psi} &= \tilde{\psi}(\xi, z, t) + \dots, \\ \bar{u} &= \tilde{u}(\xi, z, t) + \dots, \\ \bar{p} &= \xi R_1 L(z - \frac{1}{2}) + \tilde{p}(\xi, z, t) + \dots, \end{aligned} \right\} \quad (3.2)$$

with the leading terms in the temperature and pressure reflecting the fact that the initial thermal field is given by (2.10) and that the solution is centrosymmetric. Substitution into (2.1)–(2.4) gives

$$\sigma^{-1} \frac{\partial \tilde{u}}{\partial t} = -R_1(z - \frac{1}{2}) + \frac{\partial^2 \tilde{u}}{\partial z^2}, \quad (3.3)$$

$$0 = -\frac{\partial \tilde{p}}{\partial z} + R_1 \tilde{T}, \quad (3.4)$$

$$\frac{\partial \tilde{T}}{\partial t} + \tilde{u} = \frac{\partial^2 \tilde{T}}{\partial z^2}, \quad (3.5)$$

to be solved subject to the boundary conditions

$$\tilde{u} = \partial \tilde{T} / \partial z = 0 \quad (z = 0, 1) \quad (3.6)$$

and the initial conditions

$$\tilde{u} = \tilde{T} = 0 \quad (t = 0). \quad (3.7)$$

The solution for  $\tilde{u}$  is readily obtained as

$$\tilde{u} = R_1(\frac{1}{6}z^3 - \frac{1}{4}z^2 + \frac{1}{12}z) - R_1 \sum_{n=1}^{\infty} \frac{e^{-4n^2\pi^2\sigma t}}{4n^3\pi^3} \sin 2n\pi z, \quad (3.8)$$

from which it follows that

$$\tilde{\psi} = R_1 \tilde{F}(z, t), \quad (3.9)$$

where

$$\tilde{F}(z, t) = F(z) + \sum_{n=1}^{\infty} \frac{e^{-4n^2\pi^2\sigma t}}{8n^4\pi^4} (\cos 2n\pi z - 1) \quad (3.10)$$

and

$$F(z) = \frac{1}{24}z^2(1-z)^2. \quad (3.11)$$

Equation (3.5) can now be solved to obtain

$$\tilde{T} = R_1 \tilde{G}(z, t), \quad (3.12)$$

where 
$$\tilde{T}(z, t) = G(z) + \sum_{n=1}^{\infty} (G_n(z) e^{-4n^2\pi^2\sigma t} + g_n e^{-n^2\pi^2 t} \cos n\pi z). \quad (3.13)$$

Here 
$$G(z) = \frac{1}{120}z^5 - \frac{1}{48}z^4 + \frac{1}{72}z^3 - \frac{1}{1440}, \quad (3.14)$$

$$G_n(z) = \left( \frac{\sin(2n\pi\sigma^{\frac{1}{2}}(z - \frac{1}{2}))}{\sigma^{\frac{1}{2}}\cos(n\pi\sigma^{\frac{1}{2}})} - \sin 2n\pi z \right) / 16n^5\pi^5(\sigma - 1), \quad (3.15)$$

and  $g_n = 0$  for even values of  $n$  and is given by

$$g_n = \frac{4(1 - \frac{1}{12}n^2\pi^2)}{n^6\pi^6} + \frac{1}{2\pi^6} \sum_{k=1}^{\infty} \frac{1}{k^2(4k^2\sigma - n^2)(4k^2 - n^2)} \quad (3.16)$$

for odd values of  $n$ . The Prandtl-number dependence contained within the two results (3.15) and (3.16) is worthy of comment. The component of  $\tilde{T}$  associated with a typical mode  $G_N$  and generated by the transient part of the velocity field remains finite at  $\sigma = 1$  but is singular whenever the Prandtl number is equal to  $M^2/4N^2$  for any integer  $M \geq 1$ , generating a corresponding singularity in the complementary part of  $\tilde{T}$  associated with  $g_M$ . This resonance occurs when the temporal decay of the thermal field forced by  $\tilde{u}$  coincides with one of the natural modes of thermal decay. As  $\sigma \rightarrow M^2/4N^2$  the two terms involving  $G_N$  and  $g_M$  in (3.13) combine to produce a solution that remains finite at  $\sigma = M^2/4N^2$  but that contains a term proportional to  $t \exp(-M^2\pi^2 t) \cos M\pi z$ . This is the dominant part of the transient decay of  $\tilde{T}$  only when  $\sigma = \frac{1}{4}$  and  $M = N = 1$ . The pressure field can be determined from (3.4) in a straightforward manner.

It is interesting to note that the core solution found here is actually a special case, corresponding to the choice  $C = 1$ , of a family of exact solutions of (2.1)–(2.4) obtained by writing  $\bar{u} = C\tilde{u}(z, t)$ ,  $\bar{w} = 0$  and  $\bar{T} = (Cx + C^2\tilde{T}(z, t))/L$ , where  $\tilde{u}$  and  $\tilde{T}$  satisfy (3.3) and (3.5). The main results (3.8), (3.9) and (3.12) indicate that the lateral temperature variation induces a parallel flow which increases in strength with time, reaching a steady state associated with the function  $F(z)$  as  $t \rightarrow \infty$ . This flow is towards the cold endwall in the top half of the cavity and towards the hot wall in the bottom half. The fluid motion in turn generates a vertical temperature variation throughout the core region which reaches a steady-state form associated with the function  $G(z)$  as  $t \rightarrow \infty$ . In general the timescale on which this steady-state motion is achieved increases as the Prandtl number decreases, being proportional to  $\sigma^{-1}$  as  $\sigma \rightarrow 0$ . For low Prandtl numbers, any transient motion associated with setting up the initial conductive state (2.10) in the manner described in §2 would modify the solution when  $t = O(1)$  but would not affect the evolution of the flow on the longer timescale  $t = O(\sigma^{-1})$ .

In the early stages of the motion, as the fluid accelerates from rest, the velocity field is given by

$$\tilde{u} \sim \sigma R_1 t(\frac{1}{2} - z), \quad t \rightarrow 0, \quad (3.17)$$

with slip velocities of order  $t$  induced near the upper and lower boundaries. Near the lower boundary

$$\tilde{u} \sim \sigma R_1 t f(\zeta), \quad t \rightarrow 0, \quad (3.18)$$

where  $\zeta = z/(\sigma t)^{\frac{1}{2}}$  and from (3.3) and (3.6),

$$\left. \begin{aligned} f'' + \frac{1}{2}\zeta f' - f &= -\frac{1}{2}; \\ f &= 0 \quad (\zeta = 0), \quad f \rightarrow \frac{1}{2} \quad (\zeta \rightarrow \infty). \end{aligned} \right\} \quad (3.19)$$

The required solution for  $f$  is

$$f = \frac{1}{2} - \left(\frac{2}{\pi}\right)^{\frac{1}{2}} e^{-\frac{1}{8}\zeta^2} U\left(\frac{5}{2}, \zeta/\sqrt{2}\right), \quad (3.20)$$

where  $U$  is the parabolic cylinder function defined by Abramowitz & Stegun (1965, p. 686). An equal and opposite flow occurs near the upper surface of the cavity at small times.

The time-dependent core solution (3.2) does not satisfy the boundary conditions at the endwalls of the cavity, where the flow is turned. The nature of the flow near each lateral boundary is considered in the next two sections.

#### 4. End zone

The solution in the end zone at the cold wall can be expanded as

$$\left. \begin{aligned} \bar{T} &= L^{-1}T(x, z, t) + \dots \\ \bar{\psi} &= \psi(x, z, t) + \dots \end{aligned} \right\} (L \rightarrow \infty), \quad (4.1)$$

and elimination of the pressure in (2.1)–(2.4) shows that the flow is governed by the full time-dependent Boussinesq system

$$\sigma^{-1} \left( \frac{\partial \nabla^2 \psi}{\partial t} + \frac{\partial (\nabla^2 \psi, \psi)}{\partial (x, z)} \right) = \nabla^4 \psi - R_1 \frac{\partial T}{\partial x}, \quad (4.2)$$

$$\frac{\partial T}{\partial t} + \frac{\partial (T, \psi)}{\partial (x, z)} = \nabla^2 T, \quad (4.3)$$

$$\psi = \partial \psi / \partial x = T = 0 \quad \text{on} \quad x = 0, \quad (4.4)$$

$$\psi = \partial \psi / \partial z = \partial T / \partial z = 0 \quad \text{on} \quad z = 0, 1. \quad (4.5)$$

The solution must also match with that in the core, requiring that

$$\left. \begin{aligned} T &\sim x + R_1 \tilde{G}(z, t) \\ \psi &\rightarrow R_1 \tilde{F}(z, t) \end{aligned} \right\} (x \rightarrow \infty), \quad (4.6)$$

and must satisfy the initial conditions

$$T = x, \quad \psi = 0 \quad \text{at} \quad t = 0. \quad (4.7)$$

Computational solutions of this nonlinear system are described in §5. Here the structure of the solution is considered for large times and it is shown that the end zone develops two distinct parts, an inner region  $x \sim 1$  where a steady-state solution evolves and an outer region  $x \sim t^{\frac{1}{2}}$  where the flow remains time dependent as  $t \rightarrow \infty$ .

In the inner region it is anticipated that

$$\psi \rightarrow \psi_s(x, z), \quad T \rightarrow T_s(x, z) \quad \text{as} \quad t \rightarrow \infty, \quad (4.8)$$

where  $\psi_s$  and  $T_s$  are steady-state solutions of (4.2)–(4.5) such that

$$\psi_s \rightarrow R_1 F(z), \quad T_s \sim x + c + R_1 G(z), \quad x \rightarrow \infty, \quad (4.9)$$

where  $c = c(R_1, \sigma)$  is a constant whose value depends only on  $R_1$  and  $\sigma$ , and  $F$  and  $G$  are the steady-state limiting forms of  $\tilde{F}$  and  $\tilde{G}$ , as given by (3.11) and (3.14). Here it is assumed that the values of  $\sigma$  and  $R_1$  exclude the possibility of multicellular convection of the type described in the Introduction. Numerical solutions for  $\psi_s$  and  $T_s$  and the corresponding values of  $c$ , which are determined as an integral part of the solution, have been obtained for a range of values of  $\sigma$  and  $R_1$  by Wang & Daniels (1993). Since  $c$  is non-zero, the behaviour (4.9) is not consistent with the form of the outer boundary condition (4.6) for large times,

$$T \sim x + R_1 G(z), \quad \psi \rightarrow R_1 F(z). \quad (4.10)$$

The necessary adjustment occurs in an outer region where the lateral diffusion of heat is significant, allowing the form (4.10) to be attained as  $x/t^{1/2} \rightarrow \infty$ .

In the outer region the solution can be expanded for large times in the form

$$\left. \begin{aligned} \psi &= R_1 F(z) + t^{-1/2} \psi_1(z, \eta) + t^{-1} \psi_2(z, \eta) + \dots \\ T &= x + R_1 G(z) + T_0(z, \eta) + t^{-1/2} T_1(z, \eta) + t^{-1} T_2(z, \eta) + \dots \end{aligned} \right\} (t \rightarrow \infty), \quad (4.11)$$

where  $\eta = x/t^{1/2}$ . Substitution into (4.2), (4.3) gives, at order one,

$$F'''' = 1, \quad R_1 G'' + \partial^2 T_0 / \partial z^2 = R_1 F'. \quad (4.12)$$

This implies that  $\partial^2 T_0 / \partial z^2 = 0$ , and since  $\partial T_0 / \partial z = 0$  at  $z = 0$  and  $z = 1$  it follows that

$$T_0 = T_0(\eta). \quad (4.13)$$

At order  $t^{-1/2}$ ,  $\psi_1$  and  $T_1$  are found to satisfy

$$\frac{\partial^4 \psi_1}{\partial z^4} = R_1 \frac{dT_0}{d\eta}, \quad \frac{\partial^2 T_1}{\partial z^2} = \frac{\partial \psi_1}{\partial z} + R_1 F' \frac{dT_0}{d\eta}, \quad (4.14)$$

$$\text{with} \quad \psi_1 = \partial \psi_1 / \partial z = \partial T_1 / \partial z = 0 \quad \text{at} \quad z = 0, 1 \quad (4.15)$$

$$\text{so that} \quad \psi_1 = R_1 F \frac{dT_0}{d\eta}, \quad (4.16)$$

$$T_1 = 2R_1 G \frac{dT_0}{d\eta} + \tilde{T}_1(\eta), \quad (4.17)$$

where  $\tilde{T}_1$  is an unknown function of  $\eta$ .

At order  $t^{-1}$ ,  $T_2$  is found to satisfy

$$\frac{d^2 T_0}{d\eta^2} + \frac{\partial^2 T_2}{\partial z^2} = \frac{\partial \psi_2}{\partial z} + \left( \frac{\partial \psi_1}{\partial z} - \frac{1}{2} \eta \right) \frac{dT_0}{d\eta} + R_1 F' \frac{\partial T_1}{\partial \eta} - R_1 G' \frac{\partial \psi_1}{\partial \eta}, \quad (4.18)$$

$$\text{with} \quad \psi_2 = \partial \psi_2 / \partial z = \partial T_2 / \partial z = 0 \quad \text{at} \quad z = 0, 1. \quad (4.19)$$

Substitution for  $\psi_1$  and  $T_1$  from (4.16), (4.17) and integration from  $z = 0$  to  $z = 1$  using (4.15) and (4.19) shows that  $T_0$  satisfies the equation

$$(1 + 3R_1^2 Q_0) \frac{d^2 T_0}{d\eta^2} + \frac{1}{2} \eta \frac{dT_0}{d\eta} = 0, \quad (4.20)$$

$$\text{where} \quad Q_0 = \int_0^1 G'^2 dz = 1/362880. \quad (4.21)$$

The solution for  $T_0$  must match with the inner behaviour (4.9) as  $\eta \rightarrow 0$ , requiring that

$$T_0 = c \quad \text{at} \quad \eta = 0 \quad (4.22)$$

and must be consistent with the outer behaviour (4.10) as  $\eta \rightarrow \infty$ , equivalent to the requirement that

$$T_0 \rightarrow 0 \quad \text{as} \quad \eta \rightarrow \infty. \quad (4.23)$$

The relevant solution is therefore

$$T_0 = c \operatorname{erfc}(\eta/2(1 + 3R_1^2 Q_0)^{1/2}). \quad (4.24)$$

Thus the end zone spreads into the core on the scale  $x \sim t^{1/2}$  as  $t \rightarrow \infty$ , eventually modifying the solution outlined in §3. In order for the flow and heat transfer to achieve a steady-state form near each lateral wall the core temperature must rise by an amount

$cL^{-1}$  near the cold wall and fall by the same amount near the hot wall. Because of the large lateral scale of the cavity this leads to an adjustment of the temperature field across the entire core over a long timescale  $t = O(L^2)$ , to be considered in §6.

## 5. Numerical solution of the end-zone problem

Numerical solutions of the end-zone problem (4.2)–(4.7) were undertaken to confirm the behaviour outlined in §4. These were based on the use of a Dufort–Frankel multigrid method previously used to obtain steady-state solutions of the end-zone problem (Wang & Daniels 1993). This explicit finite-difference method has second-order accuracy and uses the three-level Dufort–Frankel scheme (Roache 1976) to advance the temperature and vorticity fields and a multilevel method (Brandt 1977) to solve Poisson’s equation for the stream function. An iterative method is used on the first time step and this allows the three-level scheme to be implemented on the second and subsequent time steps. The size of the time step is limited by a Courant condition and a uniform spatial mesh is used with an outer boundary at  $x = x_\infty$ , where the outer behaviour (4.6) is applied in the form

$$\partial T / \partial x = 1, \quad \psi = R_1 \tilde{F}(z, t). \quad (5.1)$$

A large value of  $x_\infty$  is needed to accommodate the outward spread of the solution with time and, in the computations reported here,  $x_\infty$  was chosen as 60. Further details of the numerical scheme are given by Wang (1992).

Contours of temperature, vorticity and stream function are shown in figures 1–4 for  $R_1 = 500$ ,  $\sigma = 0.733$  and various times up to  $t = 50$ . The temperature field starts from the linear form  $T = x$  at  $t = 0$  and gradually develops the vertical gradient associated with the anticipated form at large times. The fluid velocity increases in amplitude, driven by the lateral temperature gradient, and the position of maximum stream function moves from the core region to a position near the wall as  $t \rightarrow \infty$ . Eventually the solution near the wall attains the steady-state form previously reported by Wang & Daniels (1993). However, farther from the wall, the solution continues to change with time, as shown by profiles of  $T - x$  on the centreline  $z = \frac{1}{2}$  for successive times in figure 5. Near the wall the observed maximum is associated with the behaviour

$$T - x \sim c \quad (1 \ll x \ll t^{\frac{1}{2}}), \quad (5.2)$$

the solution approaching the value  $c(R_1, \sigma) = c(500, 0.733) \approx 0.28$  as  $t \rightarrow \infty$ . At large distances the solution approximates the form given by (4.24). A rough estimate of the decay of the complementary error function suggests that the outer behaviour is reached close to where its argument is 2, equivalent to

$$x \sim 4t^{\frac{1}{2}}(1 + 3R_1^2 Q_0)^{\frac{1}{2}}. \quad (5.3)$$

For  $R_1 = 500$  this gives  $x \sim 7.0t^{\frac{1}{2}}$ , which is in good agreement with the computed solution shown in figure 5. As  $t$  increases, the numerical solution can in fact no longer be accommodated without increasing  $x_\infty$  beyond 60, leading to spurious behaviour in the region  $x \geq 40$ .

## 6. Long-timescale evolution

As the two end zones spread into the core, the solution there is modified when the lateral scale (5.3) is comparable with the cavity width  $L$ , which occurs when  $t = O(L^2)$ .

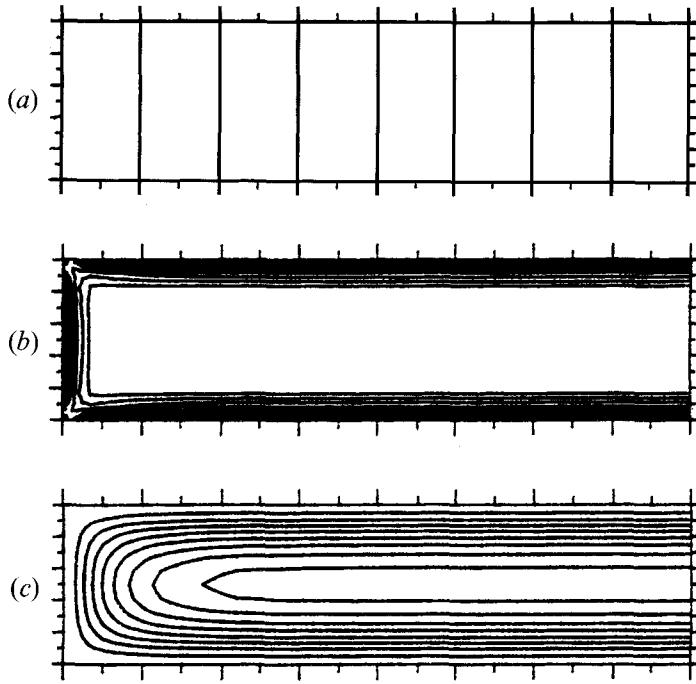


FIGURE 1. Contours of (a) temperature, (b) vorticity, (c) stream function, at intervals 0.5, 2.5 and 0.03 respectively, in the end zone for  $R_1 = 500$  and  $\sigma = 0.733$  at  $t = 0.005$  using a  $750 \times 12$  computational grid. Only the region  $0 \leq x \leq 4$ ,  $0 \leq z \leq 1$  is shown.

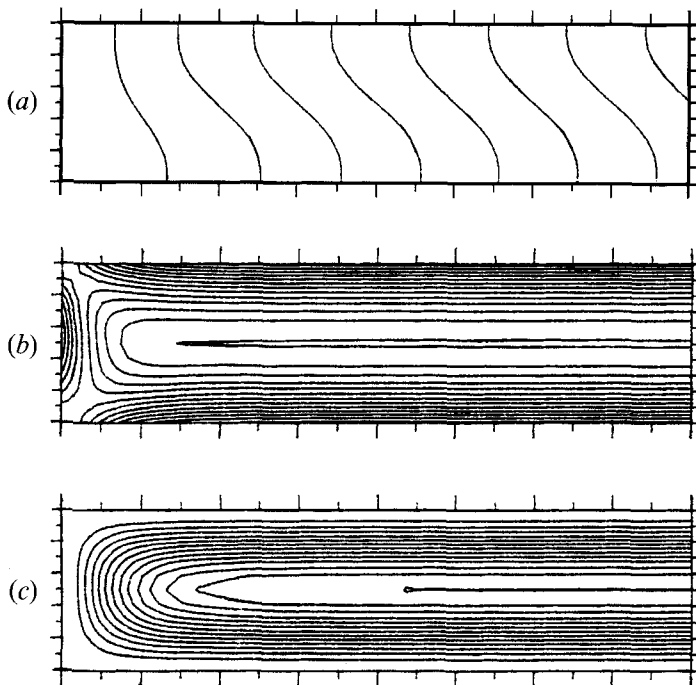


FIGURE 2. Contours of (a) temperature, (b) vorticity, (c) stream function, at intervals 0.5, 5 and 0.1 respectively, in the end zone for  $R_1 = 500$  and  $\sigma = 0.733$  at  $t = 0.2$ .

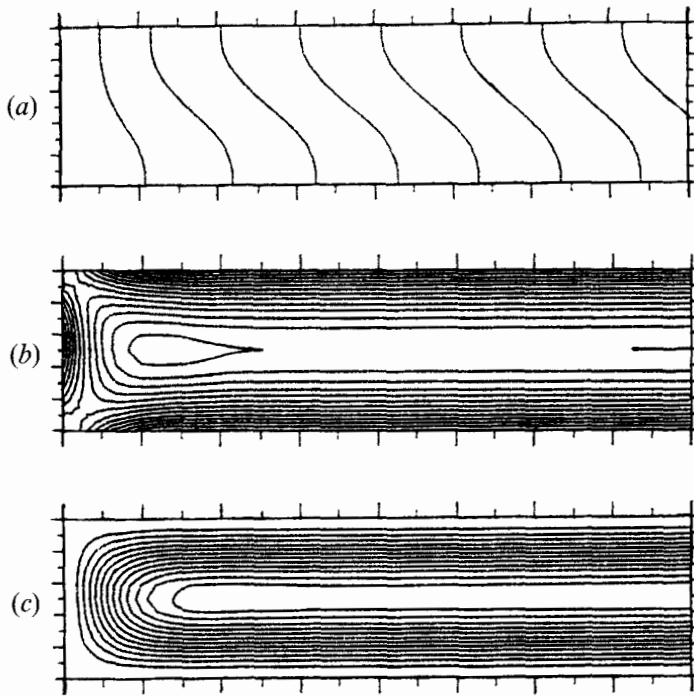


FIGURE 3. Contours of (a) temperature, (b) vorticity, (c) stream function, at intervals 0.5, 5 and 0.1 respectively, in the end zone for  $R_1 = 500$  and  $\sigma = 0.733$  at  $t = 5$ .

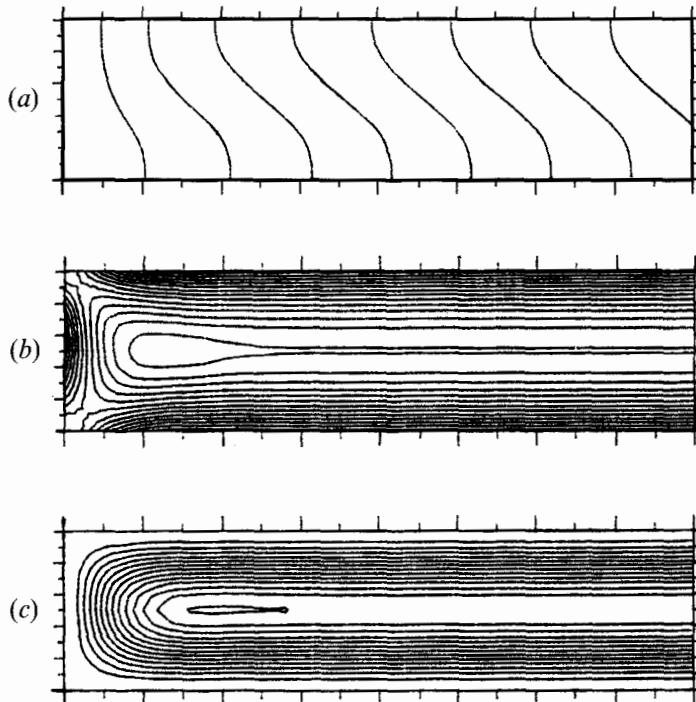


FIGURE 4. Contours of (a) temperature, (b) vorticity, (c) stream function, at intervals 0.5, 5 and 0.1 respectively, in the end zone for  $R_1 = 500$  and  $\sigma = 0.733$  at  $t = 50$ .

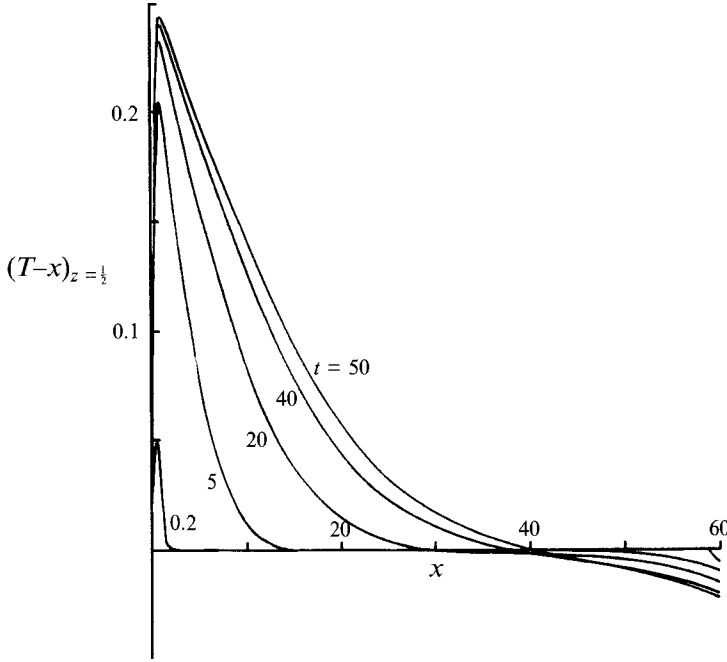


FIGURE 5. The function  $T-x$  at  $z = \frac{1}{2}$  within the end zone for  $R_1 = 500$ ,  $\sigma = 0.733$  and various times.

In order to determine the solution in the core on this long timescale, the solution there is expanded in the form

$$\left. \begin{aligned} \bar{T} &= \xi + L^{-1}\bar{T}_1(\xi, z, \tau) + L^{-2}\bar{T}_2(\xi, z, \tau) + L^{-3}\bar{T}_3(\xi, z, \tau) + \dots \\ \bar{\psi} &= R_1 F(z) + L^{-1}\bar{\psi}_1(\xi, z, \tau) + L^{-2}\bar{\psi}_2(\xi, z, \tau) + \dots \end{aligned} \right\} (L \rightarrow \infty), \quad (6.1)$$

where  $\xi = x/L$  and  $\tau = t/L^2$ . From (2.1)–(2.4) the governing equations and boundary conditions can be written in a form identical to (4.2), (4.3) and (4.5) but with  $\psi$ ,  $T$  and  $R_1$  replaced by  $\bar{\psi}$ ,  $\bar{T}$  and  $R_1 L$  respectively. Substitution of (6.1) then leads to the following results.

At order one,  $F'''' = 1$  with  $F = F' = 0$  on  $z = 0, 1$ , consistent with the solution for  $F$  given by (3.11). At order  $L^{-1}$ ,

$$\frac{\partial^4 \bar{\psi}_1}{\partial z^4} = R_1 \frac{\partial \bar{T}_1}{\partial \xi}, \quad \frac{\partial^2 \bar{T}_1}{\partial z^2} = R_1 F', \quad (6.2)$$

with  $\bar{\psi}_1 = \partial \bar{\psi}_1 / \partial z = \partial \bar{T}_1 / \partial z = 0$  on  $z = 0, 1$ . The relevant solutions are

$$\bar{\psi}_1 = R_1 F(z) \partial A / \partial \xi, \quad (6.3)$$

$$\bar{T}_1 = R_1 G(z) + A(\xi, \tau), \quad (6.4)$$

where  $G$  is given by (3.14) and  $A(\xi, \tau)$  is an unknown function of  $\xi$  and  $\tau$ .

At order  $L^{-2}$ ,  $\bar{T}_2$  is found to satisfy

$$\frac{\partial^2 \bar{T}_2}{\partial z^2} = R_1 F' \frac{\partial \bar{T}_1}{\partial \xi} + \frac{\partial \bar{\psi}_1}{\partial z} \quad (6.5)$$

and since  $\partial\bar{T}_2/\partial z = 0$  on  $z = 0, 1$ , this gives

$$\bar{T}_2 = 2R_1 G(z) \partial\bar{T}_1/\partial\xi + B(\xi, \tau), \quad (6.6)$$

where  $B(\xi, \tau)$  is an unknown function of  $\xi$  and  $\tau$ .

At order  $L^{-3}$ ,  $\bar{T}_3$  is found to satisfy

$$\frac{\partial^2\bar{T}_3}{\partial z^2} + \frac{\partial^2\bar{T}_1}{\partial\xi^2} = R_1 F' \frac{\partial\bar{T}_2}{\partial\xi} + \frac{\partial\bar{T}_1}{\partial\xi} \frac{\partial\bar{\psi}_1}{\partial z} + \frac{\partial\bar{T}_1}{\partial\tau} - \frac{\partial\bar{\psi}_1}{\partial\xi} \frac{\partial\bar{T}_1}{\partial z} + \frac{\partial\bar{\psi}_2}{\partial z}, \quad (6.7)$$

with  $\partial\bar{T}_3/\partial z = 0$  on  $z = 0, 1$ . Substitution of (6.3), (6.4) and (6.6) into (6.7) and integration from  $z = 0$  to  $z = 1$  yields an equation for  $A(\xi, \tau)$ :

$$\frac{\partial A}{\partial\tau} = (1 + 3R_1^2 Q_0) \frac{\partial^2 A}{\partial\xi^2}, \quad (6.8)$$

where  $Q_0$  is given by (4.21).

The solution for  $\bar{T}_1$  must match with that in each end zone, where the relevant leading-order solution on the long timescale  $t = O(L^2)$  is the steady-state solution associated with the inner forms  $\psi_s(x, z)$  and  $T_s(x, z)$  given by (4.8). Thus

$$A(0, \tau) = c \quad (6.9)$$

and similarly for the other end of the cavity

$$A(1, \tau) = -c. \quad (6.10)$$

As  $\tau \rightarrow 0$  the solution must match with that given by (3.2) as  $t \rightarrow \infty$ , which requires

$$A(\xi, 0) = 0, \quad 0 < \xi < 1. \quad (6.11)$$

The solution for  $A$  is

$$A = c(1 - 2\xi) - \sum_{n=1}^{\infty} \frac{2c}{n\pi} e^{-4n^2\pi^2 Q\tau} \sin 2n\pi\xi, \quad (6.12)$$

where  $Q = 1 + 3R_1^2 Q_0$ . In summary, the core solution for  $\tau > 0$  takes the form

$$\left. \begin{aligned} \bar{T} &= \xi + L^{-1} \left\{ R_1 G(z) + c(1 - 2\xi) - \sum_{n=1}^{\infty} \frac{2c}{n\pi} e^{-4n^2\pi^2 Q\tau} \sin 2n\pi\xi \right\} + O(L^{-2}), \\ \bar{\psi} &= R_1 F(z) - 2L^{-1} R_1 F(z) c \left\{ 1 + 2 \sum_{n=1}^{\infty} e^{-4n^2\pi^2 Q\tau} \cos 2n\pi\xi \right\} + O(L^{-2}). \end{aligned} \right\} \quad (6.13)$$

As  $\tau \rightarrow \infty$ , this solution approaches the steady-state form previously identified by Daniels *et al.* (1987). The effect of the lateral boundaries is to produce a reaction in the core region which, as  $\tau$  increases, reduces the lateral temperature gradient from  $\partial T/\partial x \sim L^{-1}$  to  $L^{-1}(1 - 2cL^{-1})$ . The horizontal flow across the core is reduced by a similar factor.

## 7. Discussion

The preceding theory can be extended to a more general class of initial profiles of the form

$$\bar{T} = \left(1 - \frac{a}{L}\right) \frac{x}{L} + \frac{a}{2L}, \quad \bar{\psi} = 0 \quad \text{at} \quad t = 0, \quad (7.1)$$

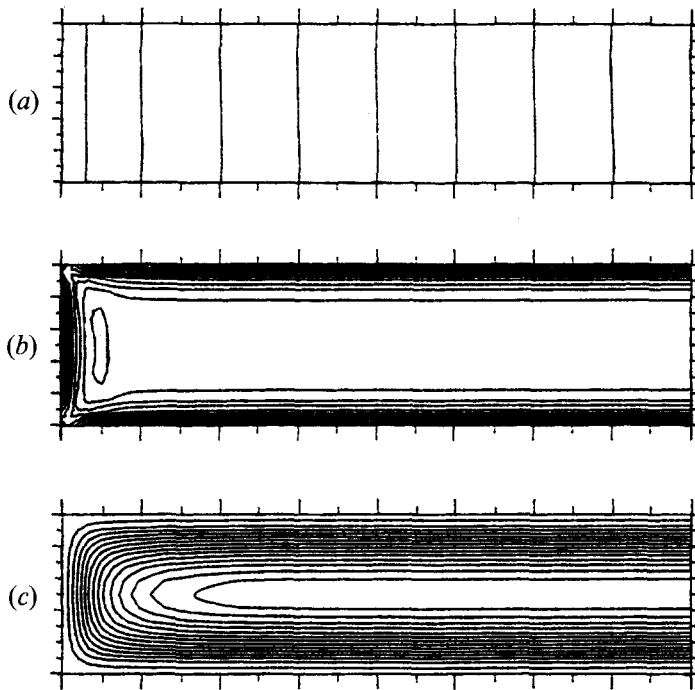


FIGURE 6. Contours of (a) temperature, (b) vorticity, (c) stream function, at intervals 0.5, 2.5 and 0.03 respectively, in the end zone for  $R_1 = 500$ ,  $\sigma = 0.733$  and  $a = 1$  at  $t = 0.01$ , using a  $750 \times 12$  computational grid.

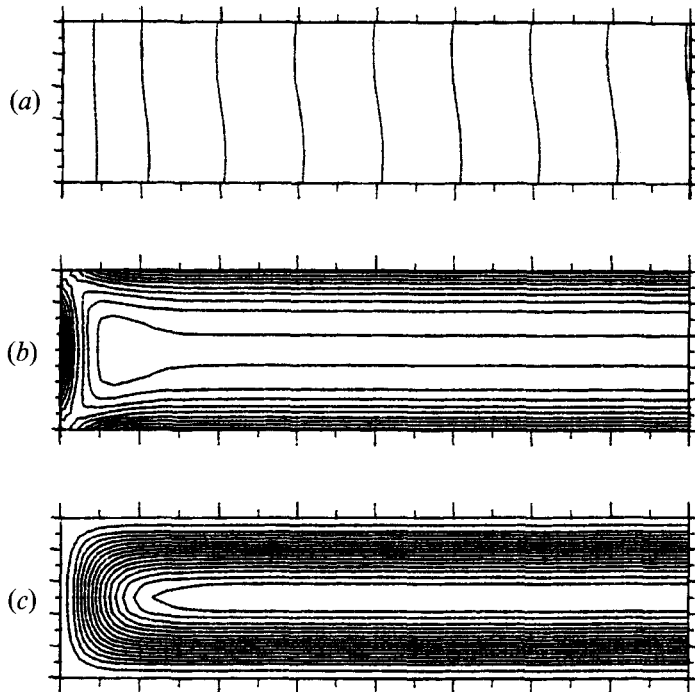


FIGURE 7. Contours of (a) temperature, (b) vorticity, (c) stream function, at intervals 0.5, 5 and 0.05 respectively, in the end zone for  $R_1 = 500$ ,  $\sigma = 0.733$  and  $a = 1$  at  $t = 0.02$ .

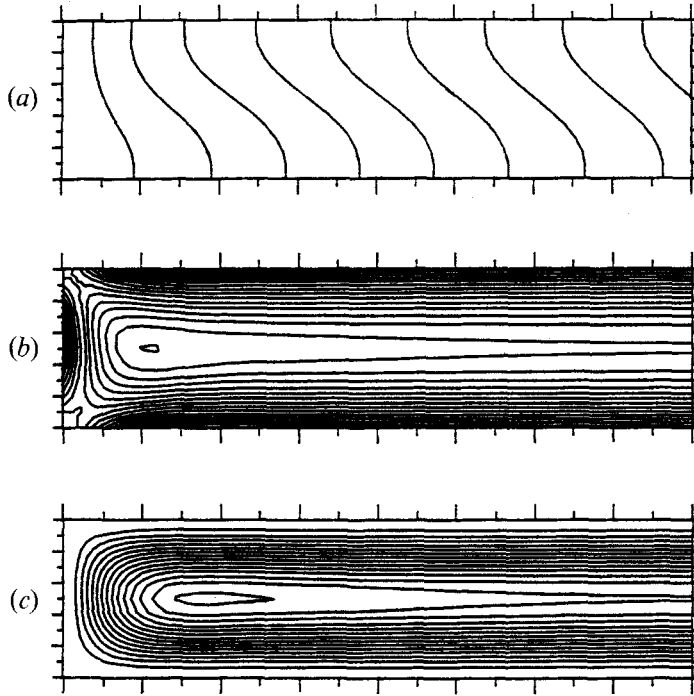


FIGURE 8. Contours of (a) temperature, (b) vorticity, (c) stream function, at intervals 0.5, 5 and 0.1 respectively, in the end zone for  $R_1 = 500$ ,  $\sigma = 0.733$  and  $a = 1$  at  $t = 0.5$ .

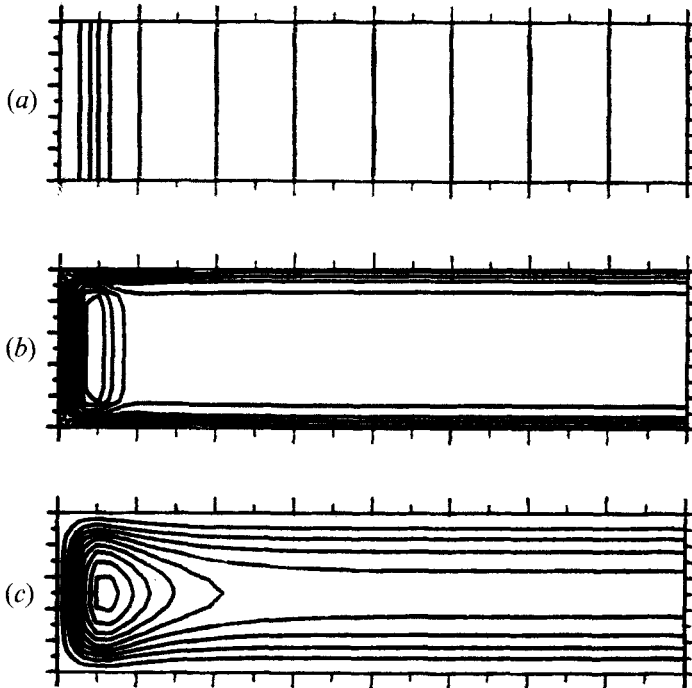


FIGURE 9. Contours of (a) temperature, (b) vorticity, (c) stream function, at intervals 0.5, 5 and 0.05 respectively, in the end zone for  $R_1 = 500$ ,  $\sigma = 0.733$  and  $a = 4$  at  $t = 0.005$ , using a  $750 \times 12$  computational grid.

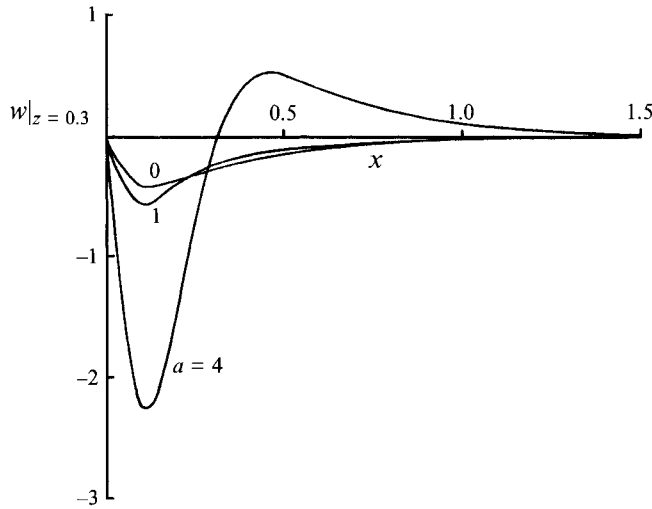


FIGURE 10. The vertical velocity,  $w$ , in the end zone at  $z = 0.3$  and  $t = 0.005$  for  $R_1 = 500$ ,  $\sigma = 0.733$  and initial conditions corresponding to  $a = 0, 1$  and  $4$ .

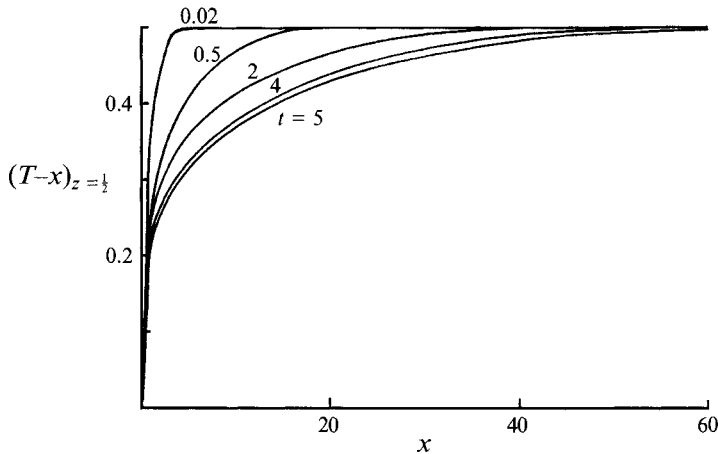


FIGURE 11. The function  $T-x$  at  $z = \frac{1}{2}$  within the end zone for  $R_1 = 500$ ,  $\sigma = 0.733$  and various times, with the initial condition corresponding to  $a = 1$ .

where  $a$  is a finite constant. The case  $a = 0$  corresponds to the situation considered in §§2–6, while increasing values of  $a$  correspond to a weaker initial temperature gradient with a jump in temperature at  $t = 0$  at each endwall. In such cases the initial evolution is less gradual and indeed the case  $a = L$  would correspond to starting from a uniform temperature  $\bar{T} = \frac{1}{2}$  throughout the cavity with the motion generated by the sudden change in temperature to  $\bar{T} = 0$  and  $\bar{T} = 1$  at the endwalls. This leads to initial motions near the ends which for large values of  $a$  take the form of wall jets generated by the sudden heating. Provided  $a$  is finite the preceding analysis can easily be extended to incorporate such effects. The core solution for  $t = O(1)$  becomes

$$\left. \begin{aligned} \bar{T} &= \xi + L^{-1}(\frac{1}{2}a - a\xi + R_1 \tilde{G}(z, t)) + O(L^{-2}), \\ \bar{\psi} &= R_1(1 - aL^{-1}) \tilde{F}(z, t) + O(L^{-2}), \end{aligned} \right\} \quad (7.2)$$

where  $\tilde{G}$  and  $\tilde{F}$  are the functions defined in (3.10) and (3.13). This is a straightforward

generalization of the previous solution which for  $a > 0$  is modified by the slightly reduced lateral temperature gradient and horizontal flow associated with the new initial profile. For  $t = O(L^2)$  this simply provides a new initial profile for the amplitude function  $A$ , resulting in a core solution for  $\tau > 0$

$$\left. \begin{aligned} \bar{T} &= \xi + L^{-1} \left( R_1 G(z) + c(1 - 2\xi) + \sum_{n=1}^{\infty} \frac{a - 2c}{n\pi} e^{-4n^2\pi^2 Q\tau} \sin 2n\pi\xi \right) + O(L^{-2}), \\ \bar{\psi} &= R_1 F(z) - 2L^{-1} R_1 F(z) \left( c + (2c - a) \sum_{n=1}^{\infty} e^{-4n^2\pi^2 Q\tau} \cos 2n\pi\xi \right) + O(L^{-2}), \end{aligned} \right\} \quad (7.3)$$

which approaches the previous steady-state solution as  $\tau \rightarrow \infty$ .

There is some interest, however, in the manner in which the end-zone flow develops, particularly for large values of  $a$ . The end-zone problem for  $t = O(1)$  is as stated in (4.2)–(4.7) except that the initial profile is now

$$T = x + \frac{1}{2}a, \quad \psi = 0 \quad \text{at} \quad t = 0 \quad (7.4)$$

and the outer condition (4.6) is replaced by

$$\left. \begin{aligned} T &\sim x + \frac{1}{2}a + R_1 \tilde{G}(z, t) \\ \psi &\rightarrow R_1 \tilde{F}(z, t) \end{aligned} \right\} \quad (x \rightarrow \infty). \quad (7.5)$$

Numerical solutions of this problem were obtained for  $a = 1$  and  $a = 4$  with  $R_1 = 500$  and  $\sigma = 0.733$ . Figures 6–8 show contours of the temperature, vorticity and stream function at several times, for  $a = 1$ . During the early stages of the motion the flow contains stronger horizontal gradients near the wall than in the case  $a = 0$  but the additional effect weakens rapidly as time progresses. For higher values of  $a$  the endwall effect is more pronounced. In figure 9, for  $a = 4$ , the contours indicate a strong nonlinearity near the wall, with a local circulation generated by the sudden heating at  $t = 0$ . This is clearly shown in figure 10 by profiles of the vertical velocity  $w$  near the wall for different values of  $a$ , indicating a jet-like motion for  $a = 4$ .

Figure 11 shows how the new initial profile with  $a = 1$  affects the evolution of  $T - x$  along the centreline of the end zone, in contrast to the result obtained for  $a = 0$  in figure 5. For  $x \gg l^{\frac{1}{2}} \gg 1$ ,  $T - x$  must now approach the value  $\frac{1}{2}a = \frac{1}{2}$  while for  $1 \ll x \ll l^{\frac{1}{2}}$  the plateau value  $c \approx 0.28$  must emerge as  $t \rightarrow \infty$ . This is consistent with the behaviour observed in figure 11. The outer section where  $x \sim l^{\frac{1}{2}}$  eventually develops into part of the core solution on the long timescale  $t = O(L^2)$  which then adjusts to the steady-state form  $\bar{T} \sim \xi + L^{-1}c(1 - 2\xi)$  on  $z = \frac{1}{2}$ , independent of  $a$ , when  $\tau = L^{-2}t \gg 1$ .

In the present paper, the evolution of thermally driven shallow cavity flows from a motionless state has been considered for Rayleigh numbers,  $R$ , of the same order of magnitude as the aspect ratio. For the class of initial temperature profiles considered here, the evolution consists of two main stages: an initial stage in which the main fluid circulation is established in both the core and end regions of the cavity, and a second stage in which the core motion and temperature field are finely adjusted by the reaction produced within each end zone. The long timescale on which the steady state finally evolves has an  $e$ -folding value  $\tau = 1/4\pi^2(1 + 3R_1^2 Q_0)$ , equivalent to a dimensional timescale

$$t^* = l^2/4\pi^2\kappa(1 + 3R_1^2 Q_0), \quad (7.6)$$

where  $R_1 = R/L$ ,  $Q_0 = 1/362880$ ,  $l$  is the length of the cavity and  $\kappa$  is the thermal diffusivity of the fluid. Thus for a laboratory experiment with water in a cavity of

length  $l = 100$  cm, height  $h = 1$  cm and subject to a temperature differential of  $10^\circ\text{C}$ , the scaled Rayleigh number  $R_1$  is approximately 923 and the timescale (7.6) is 6.25 hours, indicating the substantial time needed to achieve a steady state. For flows evolving from a motionless state at uniform temperature, the results obtained for non-zero values of  $a$  give an indication of how the solution will develop. In particular, sudden heating near the lateral walls will produce jet-like motion there which will subsequently diffuse into the cavity as the main horizontal thermal gradient is established on a timescale  $t$  of order  $L^2$ . The evolution in this case corresponds to setting  $a$  equal to  $L$ , which is outside the scope of the present asymptotic analysis, but it is hoped to consider such strongly nonlinear evolutions in future work.

## REFERENCES

- ABRAMOWITZ, M. & STEGUN, I. A. 1965 *Handbook of Mathematical Functions*. Dover.
- BEJAN, A. & ROSSIE, A. N. 1981 Natural convection in a horizontal duct connecting two fluid reservoirs. *J. Heat Transfer* **103**, 108.
- BOYACK, B. E. & KEARNEY, D. W. 1972 Heat transfer by laminar natural convection in low aspect ratio cavities. *ASME Paper 72-HT-2*.
- BRANDT, A. 1977 Multi-level adaptive solutions to boundary-value problems. *Math. Comput.* **31**, 333.
- CORMACK, D. E., LEAL, L. G. & IMBERGER, J. 1974 Natural convection in a shallow cavity with differentially heated end walls. Part 1. Asymptotic theory. *J. Fluid Mech.* **65**, 209.
- DANIELS, P. G. 1993 High Rayleigh number thermal convection in a shallow laterally heated cavity. *Proc. R. Soc. Lond. A* **440**, 273.
- DANIELS, P. G., BLYTHE, P. A. & SIMPKINS, P. G. 1987 Onset of multicellular convection in a shallow laterally heated cavity. *Proc. R. Soc. Lond. A* **411**, 327.
- GILL, A. E. 1966 The boundary layer regime for convection in a rectangular cavity. *J. Fluid Mech.* **26**, 515.
- HART, J. E. 1972 Stability of thin non-rotating Hadley circulations. *J. Atmos. Sci.* **29**, 687.
- HART, J. E. 1983a Low Prandtl number convection between differentially heated end walls. *Intl J. Heat Mass Transfer* **26**, 1069.
- HART, J. E. 1983b A note on the stability of low-Prandtl-number Hadley circulations. *J. Fluid Mech.* **132**, 271.
- HURLE, D. T. J., JAKEMAN, E. & JOHNSON, C. P. 1974 Convective temperature oscillations in molten gallium. *J. Fluid Mech.* **64**, 565.
- IVEY, G. N. 1984 Experiments on transient natural convection in a cavity. *J. Fluid Mech.* **144**, 389.
- KUO, H. P. & KORPELA, S. A. 1988 Stability and finite amplitude natural convection in a shallow cavity with insulated top and bottom and heated from a side. *Phys. Fluids* **31**, 33.
- PATTERSON, J. C. & ARMFIELD, S. W. 1990 Transient features of natural convection in a cavity. *J. Fluid Mech.* **219**, 469.
- PATTERSON, J. C. & IMBERGER, J. 1980 Unsteady natural convection in a rectangular cavity. *J. Fluid Mech.* **100**, 65.
- ROACHE, P. J. 1976 *Computational Fluid Dynamics*. New Mexico: Hermosa.
- SCHLADOW, S. G., PATTERSON, J. C. & STREET, R. L. 1989 Transient flow in a side-heated cavity at high Rayleigh number: a numerical study. *J. Fluid Mech.* **200**, 121.
- WANG, P. 1992 Thermal convection in slender laterally heated cavities. Ph.D. thesis, City University.
- WANG, P. & DANIELS, P. G. 1993 Numerical solutions for the flow near the end of a shallow laterally heated cavity. *J. Engng Maths* (to appear).